Chemical Engineering Journal 466 (2023) 143056

Contents lists available at ScienceDirect

Chemical Engineering Journal

journal homepage: www.elsevier.com/locate/cej

A separation MOF with O/N active sites in nonpolar pore for One-step C_2H_4 purification from C_2H_6 or C_3H_6 mixtures

Yong-Zhi Li [a], Gang-Ding Wang [b], Rajamani Krishna [c], Qing Yin [a], Danyang Zhao [a], Jiqiu Qi [a], Yanwei Sui [a,*], Lei Hou [b,*]

[a] School of Materials and Physics, China University of Mining and Technology, Xuzhou 221116, PR China
[b] Key Laboratory of Synthetic and Natural Functional Molecule of the Ministry of Education, College of Chemistry & Materials Science, Northwest University, Xi'an 710069, PR China
[c] Van 't Hoff Institute for Molecular Sciences, University of Amsterdam 1098 XH Amsterdam, The Netherlands

ARTICLE INFO

Keywords:
Metal-organic framework
Crystal structure
Ethylene purification
MTO product separation
C_2H_6/C_2H_4 separation

ABSTRACT

Here, a 2-fold interpenetrated metal–organic framework (MOF) was synthesized by imidazole derivative and carboxyl co-ligands, which features nonpolar pore environment with accessible N/O sorption sites, resulting in the suitable pore sizes (8.78 Å × 11.45 Å) to optimally interact with C_2H_6 and C_3H_6 compared to C_2H_4. The C_3H_6- and C_2H_6-selective phenomena were rigorously studied by combining pure-component sorption isotherms, ideal adsorbed solution theory (IAST) calculations, molecular simulations and breakthrough curves. The MOF exhibits high C_3H_6 uptake (53.6 $cm^3\ g^{-1}$ at 10 kPa and 298 K) and benchmark C_3H_6/C_2H_4 selectivity (17.1), surpassing all of the reported porous materials for C_3H_6/C_2H_4 separation. Molecular simulations revealed both nonpolar pore environment and accessible O/N sites synergistically "match" better with C_3H_6 and C_2H_6 to provide stronger multiple interactions than C_2H_4. Experimental breakthrough curves and transient breakthrough simulations revealed that the MOF not only can realize one-step C_2H_4 purification (purity ≥ 99.9%) from various ratios of C_2H_6/C_2H_4 and C_3H_6/C_2H_4 mixtures with great recyclability, but also greatly increase the purity of C_3H_6 (such as from 28.5% to 87.7% for 2/5 C_3H_6/C_2H_4 mixture).

1. Introduction

Light olefins, including ethylene (C_2H_4) and propylene (C_3H_6) are the major chemical feedstock for the synthesis of polymers (e.g., polystyrene, polyvinyl chloride, polystyrene, polypropylene, polyethylene) and other bulk chemical commodities [1–3], with the predicted worldwide production were more than 200 and 130 million tons in 2023, respectively, exceeding any other organic chemical [4–5]. Within the petrochemical industry, C_3H_6 and C_2H_4 are primarily obtained by methanol-to-propylene (MTO) technology and thermal decomposition of ethane (C_2H_6), respectively: the MTO process mainly produces C_3H_6 of 20.9 wt% and C_2H_4 of 51.1 wt%, and the trace unreacted C_2H_6 (5%-9%) as the impurity exists in the ethane dehydrogenation product [6–9]. The high purity of C_3H_6 and C_2H_4 are essential for the manufacture of advanced fine chemicals, thus separation of C_2H_6/C_2H_4 mixtures and MTO products (C_3H_6/C_2H_4) to obtain the pure C_2H_4 and C_3H_6 are urgently needed but remain a huge challenge owing to the similar physical and chemical properties of light hydrocarbons (Scheme S1). Currently, the light olefin/paraffin separation heavily relies on the high energy footprints heat-driven cryogenic distillation process, which accounts for ca. 0.3% of the global energy demand [10–12]. To this end, developing non-thermal driven separation technique with low carbon emissions is the promising solutions to the global energy use and emissions crisis. It is well known that adsorptive separation technology based on porous adsorbents presents a viable solution to this dilemma and displays more attractive promise with the continued advancement of customized adsorbents [13–16].

Metal-organic frameworks (MOFs) as novel porous adsorbents, have shown tremendous advantages in powerful predictability and tunability on pore size and functionality, that enable them to meet the task-specific requirements of various applications [17–23], including olefin/paraffin separation. Currently, the MOFs for C_2H_6/C_2H_4 separation can be classified into C_2H_6-selective or C_2H_4-selective MOFs, in which C_2H_4-selective MOFs are capable of preferentially adsorbing C_2H_4 over C_2H_6 while C_2H_6-selective MOFs adsorb C_2H_6 over C_2H_4 [24,25]. Nevertheless, C_2H_4-selective MOFs are not desirable because the C_2H_4 product is

* Corresponding authors.
E-mail addresses: suiyanwei@cumt.edu.cn (Y. Sui), lhou2009@nwu.edu.cn (L. Hou).

https://doi.org/10.1016/j.cej.2023.143056
Received 21 February 2023; Received in revised form 5 April 2023; Accepted 16 April 2023
Available online 21 April 2023
1385-8947/© 2023 Elsevier B.V. All rights reserved.

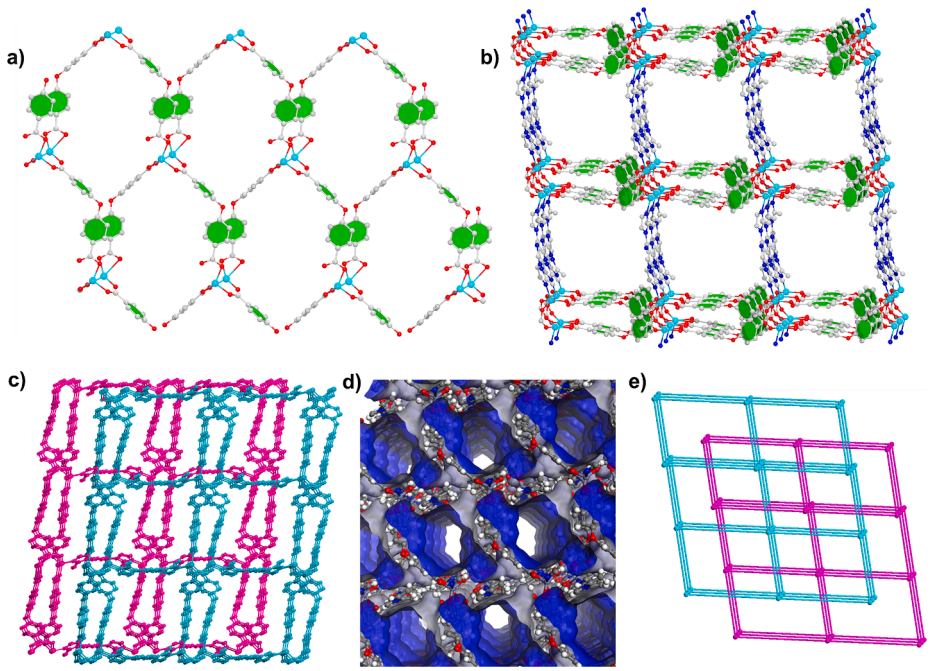

Fig. 1. a) The 2D layer; b) 3D individual framework of MOF **1** with 1D channels; c) the 2-fold interpenetrated 3D networks individually coloured; d) accessible surface representation of pores in **1** viewed along the *c* axis; e) the 2-fold interpenetrated **pcu** net.

produced by additional desorption steps, and the co-adsorption of C_2H_6 in adsorbents [26,27]. By comparison, the separation efficiency of C_2H_6-selective MOFs is remarkably increased since pure C_2H_4 can be obtained directly at the outlet by one operation process [28]. Unfortunately, only a few cases have achieved the construction of C_2H_6-selective MOFs as installing C_2H_4-binding sites such as open metal sites (OMSs) in MOFs is easier than C_2H_6-binding sites [29,30]. Furthermore, the effect of moisture to MOFs must be considered as water vapor is ubiquitous in practical applications and might result in the structure collapse or reduced gas capacity of adsorbents. Hence, the exploitation of C_2H_6-selective MOFs with high and long-term humidity stability is the desired pursuit for C_2H_4 purity goal.

Previous reports indicated that introducing inert or nonpolar functional groups in the pore walls of MOFs can prefer capturing C_2H_6, since C_2H_6 has a higher polarizability (44.7×10^{-25} cm^3) than C_2H_4 (42.5×10^{-25} cm^3), making the stronger interactions with C_2H_6 through induction and dispersion interactions [3,31,32]. Furthermore, there are also some experimental and simulation results demonstrated that implantation of hydrogen bonding acceptors such as accessible oxygen or nitrogen atoms within the pores of MOFs can form multiple hydrogen bonds between framework and C_2H_6 with more C-H bonds, enabling the construction of C_2H_6-selective MOFs [33,34]. Therefore, we envisage that the utilization of linkers containing nonpolar substituents (e.g., methyl) and metal nodes without OMSs can achieve the construction of C_2H_6-selective MOFs, while the introduction of accessible nitrogen and oxygen atoms on the linkers can improve the interaction strength for C_2H_6, and thus enhance the C_2H_6/C_2H_4 separation performance.

Inspired by these endeavors, we presented a strategy to rationally construct MOF $[Zn_2(oba)_2(dmimpym)]\cdot DMA\cdot 2H_2O\cdot 2CH_3OH$ (**1**) with nonpolar pore environment and accessible O/N adsorption sites that favour C_3H_6 and C_2H_6 over C_2H_4, through employing aromatic imidazole derivative, 4,6-di(2-methyl-imidazol-1-yl)-pyrimidine (dmimpym) and geometrically bent 4′4-oxybisbenzoic linkers (H_2oba). The methyl group functionalized pores with accessible O/N sites in the MOF **1** that on one hand preferentially adsorb C_2H_6 and C_3H_6 over C_2H_4 at ambient pressure and temperature, on the other hand improve the humid stability of the MOF because of the hydrophobic surface of the pores. The static gas adsorption isotherms, isosteric enthalpies of adsorption (Q_{st}) and IAST calculations have confirmed C_3H_6- and C_2H_6-selective behavior for MOF **1**. So the MOF **1** can separate the C_2H_6/C_2H_4 mixtures or C_3H_6/C_2H_4 mixtures to produce the pure C_2H_4 (≥99.9%) by one step, as demonstarted by simulated and experimental transient breakthrough results. Thus, together with humidity tolerance and excellent separation performance, the MOF is among the best adsorbents for C_2H_4 purification application.

2. Experimental

2.1. Materials and methods

These contents were provided in Supporting Information.

2.2. Synthesis of $[Zn_2(oba)_2(dmimpym)]\cdot DMA\cdot 2H_2O\cdot 2CH_3OH$ (1)

A mixture of 4,6-di(2-methyl-imidazol-1-yl)-pyrimidine (0.0241 g, 0.1 mmol), 4,4′-oxybis(benzoic acid) (0.0258 g, 0.1 mmol) and Zn $(NO_3)_2\cdot 6H_2O$ (0.0297 g, 0.1 mmol) was dissolved in the mixed solvent methanol (MeOH) (2 mL) and N,N'-dimethylacetamide (DMA) (4 mL) sealed in 15 mL glass vial, and heated at 95 °C for 48 h to obtain light yellow massive crystals (yield: 34%, based on $Zn(NO_3)_2\cdot 6H_2O$). The sample morphology and distribution of elements were characterized by SEM-EDX (Figure S1). Anal. Calcd for $C_{46}H_{49}N_7O_{15}Zn_2$: C, 51.59; H,4.61; N, 9.15%. Found: C, 51.54; H, 4.52; N, 9.11%.

3. Results and discussion

3.1. Crystal structure

Single-crystal X-ray diffraction reveals that the asymmetric unit of **1** consists of two Zn^{2+} isolated cations, one dmimpym linker, and two deprotonated oba^{2-} linkers with the framework formula $[Zn_2(oba)_2(dmimpym)]$, as shown in Figure S2. Zn1 is tetrahedrally coordinated by three O atoms of three oba^{2-} linkers and one N atom of dmimpym. Zn2 coordinates with one N atom belonging to dmimpym linker in the axial position and four O atoms of three oba^{2-} linkers in the equatorial plane, resulting into a square-pyramidal geometry. The

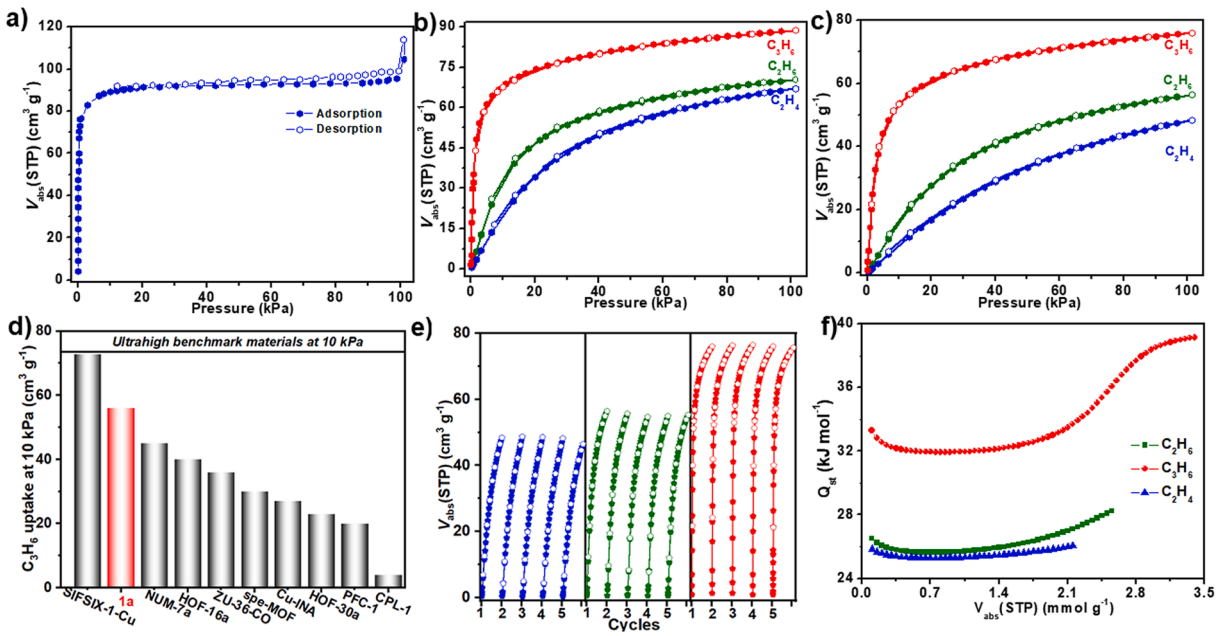

Fig. 2. a) N_2 sorption isotherm of **1a** at 77 K; b) and c) C_2H_4, C_2H_6 and C_3H_6 sorption isotherms at 273 and 298 K; d) comparisons of C_3H_6 uptakes in **1a** and top-performing adsorbents at 298 K under 10 kPa; e) repetitive C_2H_4 (blue), C_2H_6 (olive) and C_3H_6 (red) adsorption measurements at 298 K; f) the Q_{st} curves for C_2H_4, C_2H_6 and C_3H_6. (For interpretation of the references to colour in this figure legend, the reader is referred to the web version of this article.)

adjacent Zn2 and Zn1 are joined by two carboxylic acid groups of two oba^{2-} linkers to form $[Zn_2(COO)_2]$ binuclear secondary building units, and which are connected by oba^{2-} linkers to form the two-dimensional (2D) layer (Fig. 1a). As illustrated in Fig. 1b, dmimpym linkers connect the adjacent 2D layers to yield a three-dimensional (3D) pillared-layer framework. The frameworks are mutually interpenetrated to generate a 2-fold interpenetrated network (Fig. 1c), resulting in the reduction of channel void with the open sizes of ca. 8.78 Å × 11.45 Å along the *c* axis and the void volume of ~38.5% calculated by a PLATON program (Fig. 1d). Topologically, this 3D framework can be simplified as a 6-connected **pcu** topology (Fig. 1e).

3.2. Characterization

The powder X-ray diffraction (PXRD) of synthesized bulk sample matches with the simulated one obtained from the crystal structure, suggesting its great crystallinity and high phase uniformity (Figure S3). Thermo gravimetric analysis (TGA) results reveal that the MOF underwent two steps of weight loss and then was stable up to about 300 °C (Figure S4). The first weight loss about 9.6% up to 110 °C is ascribed to free MeOH and H_2O molecules (calcd. 9.4%), the subsequent weight loss from 110 to 250 °C corroborates to the expulsion of DMA solvent molecules (found 8.3%, calcd 8.1%).

3.3. Gas adsorption properties

The pore characteristics of the guest-free framework **1a** were determined by N_2 sorption experiment at 77 K. **1a** exhibited a distinct type-I N_2 sorption isotherm with the saturated adsorption amount of 113.9 $cm^3\ g^{-1}$ (Fig. 2a), and the Brunauer-Emmett-Teller (BET) surface area was fitted to be 353.8 $m^2\ g^{-1}$. The pore aperture distribution on basis of the Density Functional Theory model revealed a micropore distribution of around 10–13 Å, which is consistent with the value of crystal structure. The accessible pore surface in **1a** is mainly modified by abundant methyl groups and benzene rings, resulting in a hydrophobic and nonpolar pore environment. The water vapor adsorption isotherm at 298 K in Figure S5 shows that only 40.5 $cm^3\ g^{-1}$ water vapor was absorbed within **1a**, confirming the hydrophobicity [25]. Furthermore, **1a** can maintain the framework crystallinity and integrity after the water vapor adsorption experiment, as evidenced by PXRD results in Figure S2.

We further recorded the sorption isotherms of C_2H_4, C_3H_6 and C_2H_6 at 298 and 273 K, respectively. The adsorption capacity of **1a** for C_2H_6 and C_3H_6 are higher than that of C_2H_4 at the same temperature, show the C_3H_6- and C_2H_6-selective behavior (Fig. 2b and 2c). Under 100 kPa, the C_2H_4, C_2H_6 and C_3H_6 maximum uptakes are 48.3 $cm^3\ g^{-1}$ (2.16 mmol g^{-1}), 56.4 $cm^3\ g^{-1}$ (2.52 mmol g^{-1}) and 76.0 $cm^3\ g^{-1}$ (3.39 mmol g^{-1}) at 298 K and 67.1 $cm^3\ g^{-1}$ (2.99 mmol g^{-1}), 70.4 $cm^3\ g^{-1}$ (3.14 mmol g^{-1}) and 88.8 $cm^3\ g^{-1}$ (3.96 mmol g^{-1}) at 273 K, respectively. So C_2H_6 and C_3H_6 molecules are preferentially adsorbed into the framework through a strong adsorption affinity. Although the C_2H_6 uptake of **1a** is below that some reported C_2H_6-selective MOFs, like ScBPDC (3.42 mmol g^{-1}) [35], CPM-736 (4.02 mmol g^{-1}) [36], and Co-9-ina (3.75 mmol g^{-1}) [37], but higher than many benchmark C_2H_6-selective MOFs such as MAF-49 (1.73 mmol g^{-1}) [38] and $Cu(Qc)_2$ (1.85 mmol g^{-1}) [34]. It is worth noting that the C_3H_6 uptake (53.6 $cm^3\ g^{-1}$) of **1a** at 298 K and 10 kPa is superior to some promising porous materials, such as NUM-7a,[1] spe-MOF [39], HOF-30a [40], and CPL-1 [41] (Fig. 2d). Furthermore, the continuous C_2H_6, C_2H_4 and C_3H_6 adsorption measurements without reactivation at 298 K showed the uptake of C_2H_6, C_2H_4 and C_3H_6 no obvious decrease at least five adsorption–desorption cycles (Fig. 2e), demonstrating excellent recyclability and regeneration capability of the material. The adsorption enthalpies (Q_{st}) were determined from sorption isotherms at 298 and 273 K to appraise the interaction strengths of framework for C_2H_4, C_2H_6 and C_3H_6 (Table S3). The Q_{st} values at zero-coverage of C_3H_6, C_2H_6 and C_2H_4 were computed to be 33.3, 26.5 and 25.8 kJ mol^{-1}, respectively (Fig. 2f), corroborating that C_2H_6 and C_3H_6 have stronger affinity with the framework than C_2H_4. The Q_{st} values gradually increase at higher coverage, implying the adsorption benefits from the intermolecular interactions among the adsorbates [42–44]. It is noted the Q_{st} value for three gases are below those of MAF-49 (60.0 kJ mol^{-1}) [38], $Fe_2(O_2)$(dobdc) (66.8 kJ mol^{-1}) [14], IRMOF-8 (52.5 kJ mol^{-1}) [45], and FJI-*H*11-Me(des) (38.9 kJ mol^{-1}) [3], suggesting the low regeneration energy footprint.

To estimate the potential of **1a** for separating the mixed gases, the theoretical calculations of ideal adsorption solutions theory (IAST) for

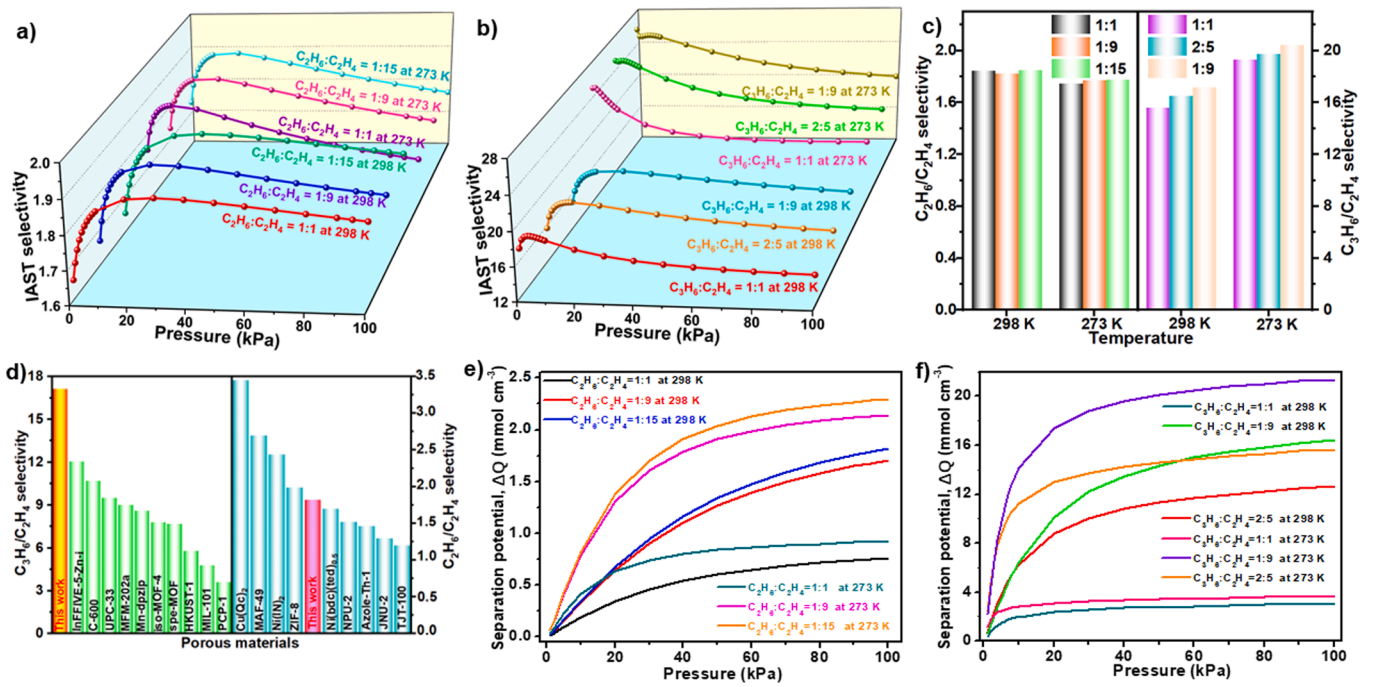

Fig. 3. IAST selectivity curves of **1a**: a) C_2H_6/C_2H_4; b) C_3H_6/C_2H_4; c) IAST selectivity values of **1a** for C_2H_6/C_2H_4 and C_3H_6/C_2H_4; d) comparison of C_3H_6/C_2H_4 (left) and C_2H_6/C_2H_4 (right) selectivities in **1a** and some benchmark materials at 298 K; e) and f) separation potential of **1a** for C_2H_6/C_2H_4 and C_3H_6/C_2H_4 mixtures at 273 and 298 K.

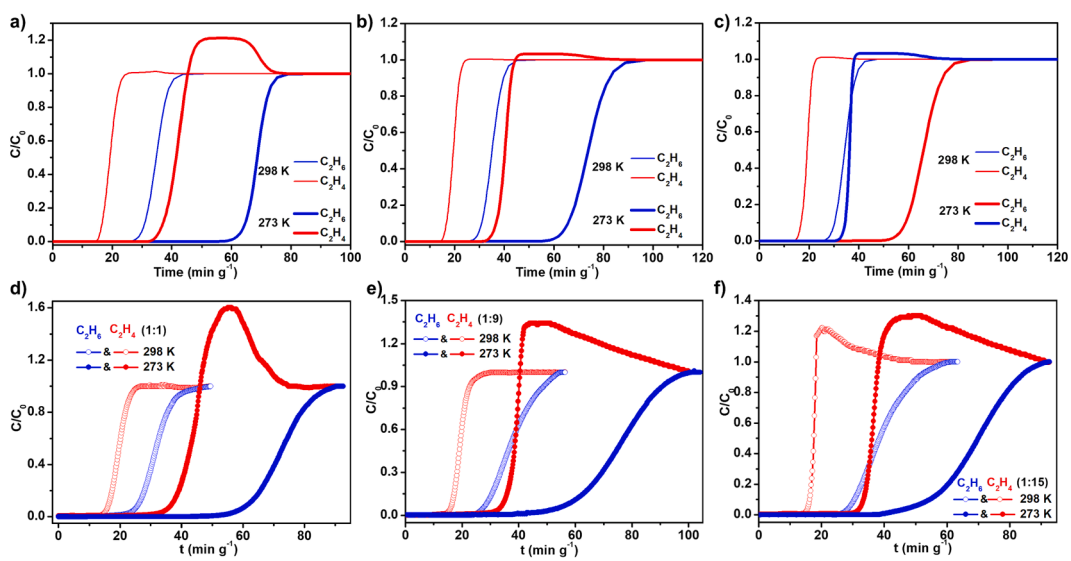

Fig. 4. a-c) Transient breakthrough simulation curves of **1a** for C_2H_6/C_2H_4 mixtures at 298 and 273 K: a) v/v, 1/1; b) v/v, 1/9; c) v/v, 1/15; d-f) experimental breakthrough curves of **1a** for C_2H_6/C_2H_4 mixtures at 298 and 273 K: d) v/v, 1/1; e) v/v, 1/9; f) v/v, 1/15.

C_2H_6/C_2H_4 (v/v; 1/15, 1/9 and 1/1) and C_3H_6/C_2H_4 (v/v; 1/1, 1/9 and 2/5) were performed to predict the adsorption selectivity at 298 and 273 K (Figure S6-S8). As displayed in Fig. 3a and 3c, the adsorption selectivities for C_2H_6/C_2H_4 mixtures of 1/1, 1/9 and 1/15 were calculated to be about 1.8, which is higher than or comparable to many C_2H_6-selective MOFs, like TJT-100 (1.2) [46], Azole-Th-1 (1.46) [47], and NPU-2 (1.52) [4], Ni(bdc)(ted)$_{0.5}$ (1.7) [48], and ZIF-8 (1.99) [49], but inferior to some benchmark MOFs, such as Cu(Qc)$_2$ (3.45) [34], MAF-49 (2.7) [38], ZJU-120a (2.74) [50], and Ni(IN)$_2$ (2.44) [51]. In addition, the selectivities for 1/1, 1/9 and 2/5 C_3H_6/C_2H_4 mixtures were 15.6/19.3, 17.1/20.4 and 16.5/19.7 at 298/273 K, respectively (Fig. 3b and 3c), which are considerably high compared to the benchmark materials for C_3H_6/C_2H_4 separation, such as C-600 (10.6) [52], UPC-33 (9.5) [53], Mn-dpzip (8.6) [54] spe-MOF (7.7) [35], and HKUST-1 (5.8) (Fig. 3d) [55].

The index to evaluate separation performance is separation potential (ΔQ), which is a combined selectivity-capacity metric introduced by Krishna [56–58]. According to the calculated ΔQ shown in Fig. 3e, the amounts of pure C_2H_4 can be recovered by **1a** reached up to 0.76/0.92, 1.70/2.14 and 1.82/2.30 mmol cm^{-3} for the 1/1, 1/9, and 1/15 C_2H_6/C_2H_4 mixtures at 298/273 K, respectively. The corresponding pure C_2H_4 values are 3.04/3.67, 12.63/15.68 and 16.43/21.39 mmol cm^{-3} for the 1/1, 2/5, and 1/9 C_3H_6/C_2H_4 mixtures at 298/273 K (Fig. 3f). These results demonstrate the potential of **1a** for one-step purification of C_2H_4

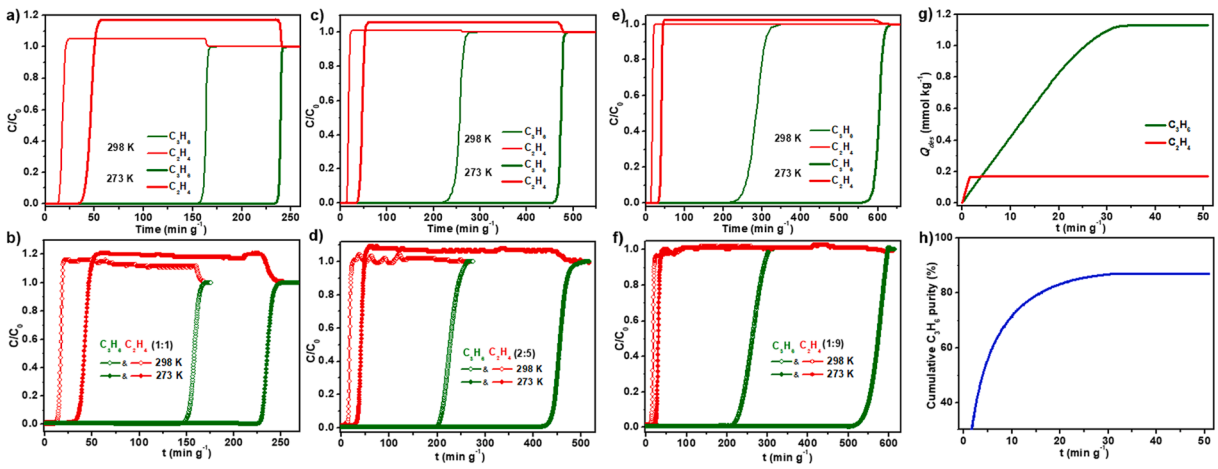

Fig. 5. a), c) and e) Transient breakthrough simulation curves of **1a** for C_3H_6/C_2H_4 mixtures at 298 and 273 K: a) v/v, 1/1; b) v/v, 2/5; c) v/v, 1/9; b), d) and f) experimental breakthrough curves of **1a** for C_3H_6/C_2H_4 mixtures at 298 and 273 K: b) v/v, 1/1; d) v/v, 2/5; f) v/v, 1/9; g) cumulative moles of C_3H_6 and C_2H_4 recovered during blowdown; h) cumulative purity of C_3H_6 recovered form **1a** during simulated counter-current blowdown operations.

from binary C_2H_6/C_2H_4 or C_3H_6/C_2H_4 mixtures.

3.4. C_2H_6/C_2H_4 separation

To verify the feasibility of C_2H_4 purification from C_2H_6/C_2H_4 mixtures, transient breakthrough simulations were conducted for **1a** in a fixed bed at 273 and 298 K and 100 kPa by using the methodology described by Krishna (see also Supporting Information) [56,58]. The simulated breakthrough results in Fig. 4a-c show that efficient separations can be achieved by **1a** for 1/1, 1/9, and 1/15 C_2H_6/C_2H_4 mixtures, wherein C_2H_4 pass through occurs first to yield the high-purity C_2H_4 and then C_2H_6 breakthrough the bed after a certain time. Next, the dynamic breakthrough experiments of C_2H_6/C_2H_4 (v/v; 1/1, 1/9, and 1/15) mixtures with Ar as the carrier gas (90%, 90% and 84%, vol %) were purged into fixed bed with total gas mixture flow rate of 5.0 mL min^{-1} at 273 and 298 K. As revealed in Fig. 4d-f, C_2H_4 can be efficiently separated from C_2H_6/C_2H_4 mixtures at two temperatures. When these three C_2H_6/C_2H_4 mixtures were passed over the fixed bed of **1a**, C_2H_4 first eluted through the fixed bed to yield a desirable pure C_2H_4 (≥99.9%) without detectable C_2H_6 signal was found (below the mass spectrometry detection limit), whereas C_2H_6 was more efficiently adsorbed in adsorbent for a certain period of time and then reached it's breakthrough point. During the breakthrough duration, C_2H_4 productivities from the outlet effluent which were determined to be 1.32/4.14, 3.29/8.47, and 5.65/13.42 L kg^{-1} for 5/5, 1/9, and 1/15 C_2H_6/C_2H_4 mixtures at 298/273 K, respectively. It is worth noting that the C_2H_4 productivity values for **1a** would be higher than the our experimental results because of industrial practice without containng inert carrier gas. The value of 5.65 L kg^{-1} C_2H_4 (≥99.9%) from 1/15 C_2H_6/C_2H_4 mixtures (partial cracked gas mixtures) is lower than some excellent materials, like [Zn(BDC)(H_2BPZ)] [8], $Fe_2(O_2)$(dobdc) [14], and TJT-100 [46], but is comparable or higher than some reported benchmark porous material (e.g., NKCOF-21 [28], HOF-76a [59], $Cu(Qc)_2$ [34], MAF-49 [38], and HIAM-102 [9]). The separation factor based on breakthrough experiments for 1/1, 1/9, and 1/15 C_2H_6/C_2H_4 mixtures were calculated to be 1.56/2.22, 1.96/2.85, and 2.67/2.65 at 298/273 K, respectively. The experimental separation factor for the C_2H_6/C_2H_4 were higher than the results predicted by IAST, indicating that **1a** more preferentially adsorb C_2H_6 than C_2H_4 in the actual C_2H_6/C_2H_4 mixtures separation process. The high C_2H_4 productivity indicates that **1a** has efficient separation performance of various ratios C_2H_6/C_2H_4 mixtures around room temperature, suggesting promising C_2H_6/C_2H_4 separation in practical

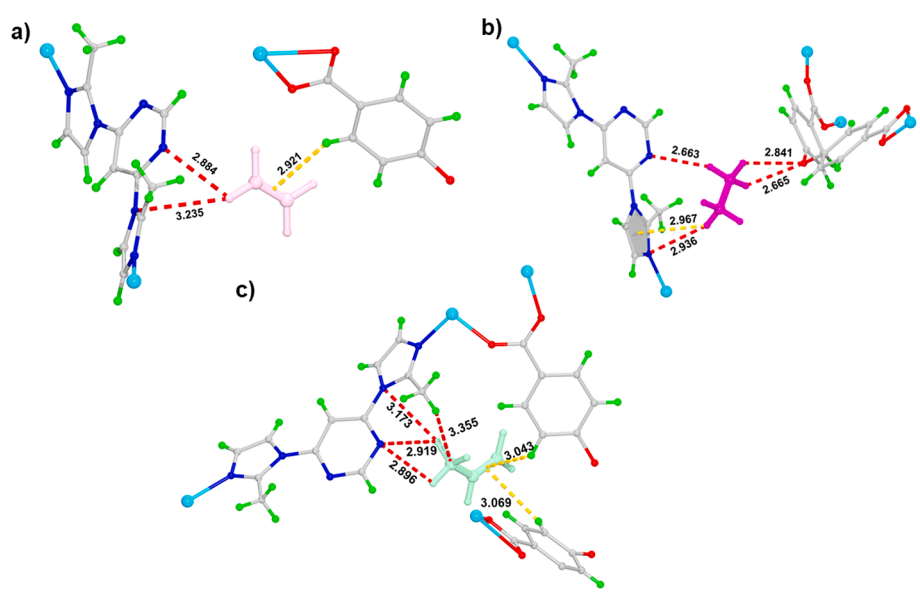

Fig. 6. Preferential bingding sites for a) C_2H_4; b) C_2H_6 and c) C_3H_6.

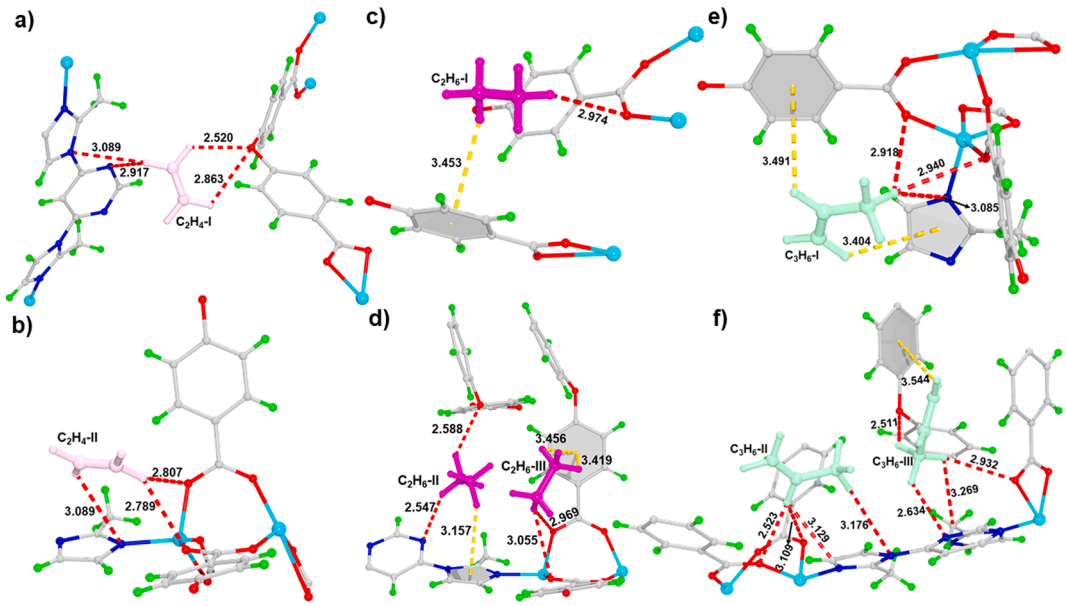

Fig. 7. Adsorption sites for a) and b) C_2H_4; c) and d) C_2H_6; e) and f) C_3H_6 in **1a** simulated at 298 K under 100 kPa.

applications. Subsequently, multiple breakthrough experiments result for C_2H_6/C_2H_4 mixtures (v/v; 1/1) exhibits that **1a** could be remained for at least five cycles without any loss in separation performance, confirming excellent separation and recovery capacity (Figure S9).

3.5. C_3H_6/C_2H_4 separation

In addition, the similar transient breakthrough simulations and experimental breakthrough curves of C_3H_6/C_2H_4 (1/1, 1/9 and 2/5; v/v) mixtures with Ar as the carrier gas (90%, 90% and 93%, vol %) were also tested to evaluate the MTO products separation performance of **1a**. As presented in Fig. 5a-f, there are excellent match between the experiments and simulations breakthrough curves, which display complete separation of these C_3H_6/C_2H_4 mixtures by **1a** at both 273 and 298 K, wherein C_2H_4 breakthrough the bed first to produce an outflow of pure C_2H_4 gas with 99.9% purity, and then C_3H_6 breaks through the fixed-bed after a substantial time lapse since it's more preferentially adsorbed in **1a**. During the breakthrough duration, the collected high-purity C_2H_4 gas are 35.62/50.01, 49.68/98.71, and 94.91/243.42 L kg^{-1} for 1/1, 2/5, and 1/9 C_3H_6/C_2H_4 mixtures at 298/273 K, respectively. And these productivity values would be higher in industrial practice without containng inert carrier gas. The C_2H_4 productivity values of **1a** are significantly higher than that of Mn-dtzip under the same conditions [54]. To estimate the possibility of **1a** for C_3H_6 purification from C_3H_6/C_2H_4 mixture, we also simulated counter-current blowdown operations for 2/5/93 C_3H_6/C_2H_4/Ar mixture at 298 K (Fig. 5g). The results showed that 87.1% C_3H_6 purity can be recovered with productivity of 1.133 mol kg^{-1} in a counter- current blowdown process (Fig. 5h). Thus, **1a** not only can produce 99.9% purity C_2H_4 by one step, but also improves the purity of C_3H_6, which implies a promising application for obtaining pure C_2H_4 and concentrate C_3H_6 simultaneously from MTO products. Furthermore, this MOF also shows great recyclability and regeneration capability for multiple C_3H_6/C_2H_4 mixtures breakthrough tests (Figure S10).

3.6. GCMC simulation

To further explore the interactions between the framework and adsorbates, the preferential binding sites for C_3H_6, C_2H_4 and C_2H_6 were firstly determined by Grand Canonical Monte Carlo (GCMC) simulations. It found that the preferential adsorption sites for three gas molecules at 298 K and 100 kPa are located at the in the similar region near the dmimpym and oba coordination fragments. As depicted in the Fig. 6a, there are only two C-H···N interactions between the H atoms of C_2H_4 and N atoms of dmimpym ligand with the H···N distances from 2.884 to 3.235 Å and one C-H···π interaction between the H atoms of phenyl ring and π center of C_2H_4 with the H···π distances of 2.921 Å. For C_2H_6 molecule, there are not only form stronger C-H···N contacts (H···N, 2.663 and 2.936 Å), C-H···π interaction (H···π, 2.967 Å), but also two C-H···O hydrogen bonds with O atoms of carbonyl group in oba ligand (H···O, 2.665 and 2.841 Å) were found (Fig. 6b). Compared to C_2H_4 and

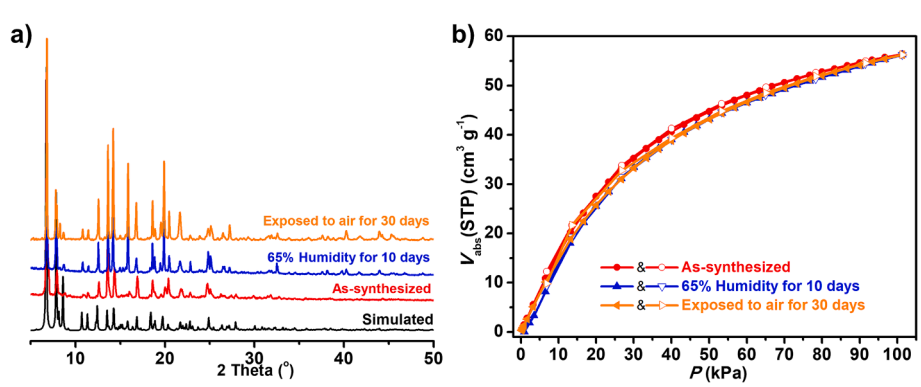

Fig. 8. a) PXRD patterns of **1** treated under different conditions; b) C_2H_6 sorption isotherms at 298 K of **1a** treated under different conditions.

C_2H_6, C_3H_6 with a larger molecular size enhances the interactions with the framework. As a consequence, one C_3H_6 molecule interacts with two H atoms of phenyl ring, one H atoms of methyl group, one imidazole N atom, one pyrimidine N atom of ligands to form more strong contacts including C-H···π/N/C interactions with the distances of 2.896–3.355 Å (Fig. 6c). The more and stronger interactions between C_2H_6/C_3H_6 and framework indicate that **1a** prefers to adsorb C_3H_6 and C_2H_6 over C_2H_4.

Furthermore, the different binding sites in **1a** for C_2H_4, C_3H_6 and C_2H_6 at 298 K under 100 kPa were further studied by GCMC simulations. As shown in Fig. 7, the MOF exhibits two adsorption sites for C_2H_4 and three important sites for C_2H_6 and C_3H_6. C_3H_6 and C_2H_6 molecules are involved in more contacts with the accessible sites of π centers from ligands and O/N atoms in framework, forming rich C-H···π interactions and C-H···O/N hydrogen bonds (Fig. 7 c,d). Notably, the methyl groups in dmimpym are also useful sites for C_3H_6 (C_3H_6-III) molecules through C-H···C interactions. By contrast, the interactions of the framework with C_2H_4 are weak due to less contact fashions (Fig. 7a,b), thus forming a priority of adsorption for C_2H_6/C_3H_6 over C_2H_4. These simulation results are consistent with the experimental selectivity of **1a** for C_2H_6/C_3H_6 over C_2H_4.

3.7. Stability test

Considering the real-industrial application, the chemical stability of **1a** toward relative humidity and air environments for a certain period of times was monitored by PXRD and gas adsorption experiments. As given in Fig. 8a, the samples were exposed to the air for 30 days and relative humidity (65%) for 10 days, it remains intact without loss of crystallinity and phase transformation, as indicated by PXRD. Subsequently, C_2H_6 adsorption isotherms at 298 K obtained after exposing to humidity and air conditions almost unchanged, demonstrating its excellent chemical stability (Fig. 8b).

4. Conclusions

In summary, we rationally designed and synthesized a robust MOF with the function of one-step C_2H_4 purification from C_2H_6/C_2H_4 and C_3H_6/C_2H_4 mixtures. During design process of MOF, on the one hand, the nonpolar pore surface composed of aromatic rings and methyl groups realized the construction of C_2H_6-selective MOF, on the other hand, the introduction of accessible O/N adsorption sites in the ligands further enhanced the interactions between the framework and C_3H_6 compared with C_2H_4. The MOF not only exhibits high C_3H_6 uptake (53.6 cm^3 g^{-1} at 10 kPa and 298 K) but also benchmark C_3H_6/C_2H_4 selectivity (17.1), surpassing all of the reported porous materials for C_3H_6/C_2H_4 separation. The MOF on one hand can efficiently separate the C_2H_4 from various ratios of C_2H_6/C_2H_4 and C_3H_6/C_2H_4 mixtures to directly produced high-purity (≥99.9%) C_2H_4 in one-step at 298 and 273 K, on the other hand, greatly increase the purity of C_3H_6 from C_3H_6/C_2H_4 mixtures. Molecular simulations revealed the nonpolar pore environment and accessible O/N sites synergistically "match" better with C_3H_6 and C_2H_6 to provide stronger multiple interactions than C_2H_4. This contribution not only reports the benchmark MOF material for C_3H_6/C_2H_4 and C_2H_6/C_2H_4 separation, but also provides some guidance to design nonpolar pore environment with accessible adsorption sites in MOFs for addressing C_2H_4 purification goal.

Declaration of Competing Interest

The authors declare that they have no known competing financial interests or personal relationships that could have appeared to influence the work reported in this paper.

Data availability

Data will be made available on request.

Acknowledgements

This work is supported by Fundamental Research Funds for the Central Universities (No. 2022QN1089) and National Natural Science Foundation of China (No. 21871220).

Appendix A. Supplementary data Additional Figures and selected bond length/angle table. CCDC 2233136 contains the supplementary crystallographic data for this paper. These data can be obtained free of charge from the Cambridge Crystallographic data Center Via http://www.ccdc.cam.ac.uk/data_request/cif.

Supplementary data to this article can be found online at https://doi.org/10.1016/j.cej.2023.143056.

References

[1] S.-Q. Yang, F.-Z. Sun, R. Krishna, Q. Zhang, L. Zhou, Y.-H. Zhang, T.-L. Hu, Propane-Trapping Ultramicroporous Metal-Organic Framework in the Low-Pressure Area toward the Purification of Propylene, ACS Appl. Mater. Interfaces 13 (2021) 35990–35996.
[2] Y. Jiang, J. Hu, L. Wang, W. Sun, N. Xu, R. Krishna, S. Duttwyler, X. Cui, H. Xing, Y. Zhang, Comprehensive Pore Tuning in an Ultrastable Fluorinated Anion Cross-Linked Cage-Like MOF for Simultaneous Benchmark Propyne Recovery and Propylene Purification, Angew. Chem. Int. Ed. 61 (2022) e202200947.
[3] Z. Di, C. Liu, J. Pang, S. Zou, Z. Ji, F. Hu, C. Chen, D. Yuan, M. Hong, M. Wu, A Metal-Organic Framework with Nonpolar Pore Surfaces for the One-Step Acquisition of C_2H_4 from a C_2H_4 and C_2H_6 Mixture, Angew. Chem. Int. Ed. 61 (2022) e202210343.
[4] J. Zhou, T. Ke, X. Zhu, B. Jin, Z. Bao, Z. Zhang, Y. Yang, Q. Ren, Q. Yang, Combination of Low-Polar and Polar Binding Sites in Aliphatic MOFs for the Efficient C_2H_6/C_2H_4 Separation, ACS Appl. Mater. Interfaces 15 (2023) 3387–3394.
[5] P. Hu, J. Hu, H. Liu, H. Wang, J. Zhou, R. Krishna, H. Ji, Quasi-Orthogonal Configuration of Propylene within a Scalable Metal-Organic Framework Enables Its Purification from Quinary Propane Dehydrogenation Byproducts, ACS Cent. Sci. 8 (2022) 1159–1168.
[6] W. Fan, X. Wang, X. Zhang, X. Liu, Y. Wang, Z. Kang, F. Dai, B. Xu, R. Wang, D. Sun, Fine-Tuning the Pore Environment of the Microporous Cu-MOF for High Propylene Storage and Efficient Separation of Light Hydrocarbons, ACS Cent. Sci. 5 (2019) 1261–1268.
[7] X.-H. Han, K. Gong, X. Huang, J.-W. Yang, X. Feng, J. Xie, B. Wang, Syntheses of Covalent Organic Frameworks via a One-Pot Suzuki Coupling and Schiff's Base Reaction for C_2H_4/C_3H_6 Separation, Angew. Chem. Int. Ed. 61 (2022) e202202912.
[8] G.-D. Wang, Y.-Z. Li, W.-J. Shi, L. Hou, Y.-Y. Wang, Z. Zhu, One-Step C_2H_4 Purification from Ternary $C_2H_6/C_2H_4/C_2H_2$ Mixtures by a Robust Metal-Organic Framework with Customized Pore Environment, Angew. Chem. Int. Ed. 61 (2022) e202205427.
[9] J. Liu, J. Miao, S. Ullah, K. Zhou, L. Yu, H. Wang, Y. Wang, T. Thonhauser, J. Li, A Water-Resistant Hydrogen-Bonded Organic Framework for Ethane/Ethylene Separation in Humid Environments, ACS Materials Lett. 4 (2022) 1227–1232.
[10] D.S. Sholl, R.P. Lively, Seven chemical separations to change the world, Nature 532 (2016) 435–437.
[11] K.-J. Chen, D.G. Madden, S. Mukherjee, T. Pham, K.A. Forrest, A. Kumar, B. Space, J. Kong, Q.-Y. Zhang, M.J. Zaworotkom, Synergistic sorbent separation for one-step ethylene purification from a four-component mixture, Science 366 (2019) 241–246.
[12] K. Adil, Y. Belmabkhout, R.S. Pillai, A. Cadiau, P.M. Bhatt, A.H. Assen, G. Maurin, M. Eddaoudi, Gas/vapour separation using ultra-microporous metal-organic frameworks: insights into the structure/separation relationship, Chem. Soc. Rev. 46 (2017) 3402–3430.
[13] S.J. Datta, A. Mayoral, N.M.S. Bettahalli, P.M. Bhatt, M. Karunakaran, I.D. Carja, D. Fan, P.G.M. Mileo, R. Semino, G. Maurin, O. Terasaki, M. Eddaoudi, Rational design of mixed-matrix metal-organic framework membranes for molecular separations, Science 376 (2022) 1080–1087.
[14] L. Li, R.-B. Lin, R. Krishna, H. Li, S. Xiang, H. Wu, J. Li, W. Zhou, B. Chen, Ethane/ethylene separation in a metal-organic framework with iron-peroxo sites, Science 362 (2018) 443–446.
[15] P. Zhang, L. Yang, X. Liu, J. Wang, X. Suo, L. Chen, X. Cui, H. Xing, Ultramicroporous material based parallel and extended paraffin nano-trap for benchmark olefin purification, Nat. Commun. 13 (2022) 4928.
[16] S. Zhou, O. Shekhah, A. Ramírez, P. Lyu, E. Abou-Hamad, J. Jia, J. Li, P.M. Bhatt, Z. Huang, H. Jiang, T. Jin, G. Maurin, J. Gascon, M. Eddaoudi, Asymmetric pore windows in MOF membranes for natural gas valorization, Nature 606 (2022) 706–712.
[17] H. Zeng, M. Xie, T. Wang, R.-J. Wei, X.-J. Xie, Y. Zhao, W. Lu, D. Li, Orthogonal-array dynamic molecular sieving of propylene/propane mixtures, Nature 595 (2021) 542–548.
[18] J.-B. Lin, T.T.T. Nguyen, R. Vaidhyanathan, J. Burner, J.M. Taylor, H. Durekova, F. Akhtar, R.K. Mah, O. Ghaffari-Nik, S. Marx, N. Fylstra, S.S. Iremonger, K.

W. Dawson, P. Sarkar, P. Hovington, A. Rajendran, T.K. Woo, G.K.H. Shimizu, A scalable metal-organic framework as a durable physisorbent for carbon dioxide capture, Science 374 (2021) 1464–1469.
[19] K. Wang, Y. Li, L.-H. Xie, X. Li, J.-R. Li, Construction and application of base-stable MOFs: a critical review, Chem. Soc. Rev. 51 (2022) 6417–6441.
[20] W. Lou, J. Li, W. Sun, Y. Hu, L. Wang, R.F. Neumann, M. Steiner, Z. Gu, B. Luan, Y. Zhang, Screening Hoffman-type metal organic frameworks for efficient C_2H_2/CO_2 separation, Chem. Eng. J. 452 (2023), 139296.
[21] T. Najam, N.A. Khan, S.S.A. Shah, K. Ahmad, M.S. Javed, S. Suleman, M.S. Bashir, M.A. Hasnat, M.M. Rahman, Meta-Organic Frameworks Derived Electrocatalysts for Oxygenand Carbon Dioxide Reduction Reaction, Chem. Rec. 22 (2022) e202100329.
[22] K. Ahmad, M.A. Nazir, A.K. Qureshi, E. Hussain, T. Najam, M.S. Javed, S.S.A. Shah, M.K. Tufail, S. Hussain, N.A. Khan, H.-u.-R. Shah, M. Ashfaq,, Engineering of Zirconium based metal-organic frameworks (Zr-MOFs) as efficient adsorbents, Mater. Sci. Eng. B 262 (2020), 114766.
[23] K. Ahmad, H.-U.-R. Shah, M. Ahmad, M.M. Ahmed, K. Naseem, N.N. Riaz, A. Muhammad, A. Ayub, M. Ahmad, Z. Ahmad, A. Munwar, A. Rauf, R. Hussain, M. Ashfaq, Comparative Study Between Two Zeolitic Imidazolate Frameworks as Adsorbents for Removal of Organoarsenic, As(III) and As(V) Species from Water, Brazilian, J. Anal. Chem. 9 (2020) 78–97.
[24] D. Lv, P. Zhou, J. Xu, S. Tu, F. Xu, J. Yan, H. Xi, W. Yuan, Q. Fu, X. Chen, Q. Xia, Recent advances in adsorptive separation of ethane and ethylene by C_2H_6-selective MOFs and other adsorbents, Chem. Eng. J. 431 (2022), 133208.
[25] S. Geng, E. Lin, X. Li, W. Liu, T. Wang, Z. Wang, D. Sensharma, S. Darwish, Y. H. Andaloussi, T. Pham, P. Cheng, M.J. Zaworotko, Y. Chen, Z. Zhang, Scalable Room-Temperature Synthesis of Highly Robust Ethane-Selective Meta-Organic Frameworks for Efficient Ethylene Purification, J. Am. Chem. Soc. 143 (2021) 8654–8660.
[26] D. Lv, R. Shi, Y. Chen, Y. Wu, H. Wu, H. Xi, Q. Xia, Z. Li, Selective Adsorption of Ethane over Ethylene in PCN-245: Impacts of Interpenetrated Adsorbent, ACS Appl. Mater. Interfaces 10 (2018) 8366–8373.
[27] L. Yang, Y. Wang, Y. Chen, J. Yang, X. Wang, L. Li, J. Li, Microporous metal-organic framework with specific functional sites for efficient removal of ethane from ethane/ethylene mixtures, Chem. Eng. J. 387 (2020), 124137.
[28] F. Jin, E. Lin, T. Wang, S. Geng, T. Wang, W. Liu, F. Xiong, Z. Wang, Y. Chen, P. Cheng, Z. Zhang, Bottom-Up Synthesis of 8-Connected Three-Dimensional Covalent Organic Frameworks for Highly Efficient Ethylene/Ethane Separation, J. Am. Chem. Soc. 144 (2022) 5643–5652.
[29] X.-W. Gu, J. Pei, K. Shao, H.-M. Wen, B. Li, G. Qian, Chemically Stable Hafnium-Based Metal-Organic Framework for Highly Efficient C_2H_6/C_2H_4 Separation under Humid Conditions, ACS Appl. Mater. Interfaces 13 (2021) 18792–18799.
[30] G.-D. Wang, J. Chen, Y.-Z. Li, L. Hou, Y.-Y. Wang, Z. Zhu, A robust ethane-selective metal-organic framework with nonpolar pore surface for efficient C_2H_6/C_2H_4 separation, Chem. Eng. J. 433 (2022), 133786.
[31] M. Kang, D.W. Kang, J.H. Choe, H. Kim, D.W. Kim, H. Park, C.S. Hong, A Robust Hydrogen-Bonded Metal-Organic Framework with Enhanced Ethane Uptake and Selectivity, Chem. Mater. 33 (2021) 6193–6199.
[32] X. Zhang, J.-X. Wang, L. Li, J. Pei, R. Krishna, H. Wu, W. Zhou, G. Qian, B. Chen, B. Li, A Rod-Packing Hydrogen-Bonded Organic Framework with Suitable Pore Confinement for Benchmark Ethane/Ethylene Separation, Angew. Chem. Int. Ed. 60 (2021) 10304–10310.
[33] X. Wang, Z. Niu, A.M. Al-Enizi, A. Nafady, Y. Wu, B. Aguila, G. Verma, L. Wojtas, Y.-S. Chen, Z. Li, S. Ma, Pore environment engineering in metal-organic frameworks for efficient ethane/ethylene separation, J. Mater. Chem. A 7 (2019) 13585–13590.
[34] R.-B. Lin, H. Wu, L. Li, X.-L. Tang, Z. Li, J. Gao, H. Cui, W. Zhou, B. Chen, Boosting Ethane/Ethylene Separation within Isoreticular Ultramicroporous Metal-Organic Frameworks, J. Am. Chem. Soc. 140 (2018) 12940–12946.
[35] S. Jiang, L. Li, L. Guo, C. Song, Q. Yang, Z. Zhang, Y. Yang, Q. Ren, Z. Bao, A robust ethane-trapping metal-organic framework for efficient purification of ethylene, Sci. China Chem. 64 (2021) 666–672.
[36] H. Yang, Y. Wang, R. Krishna, X. Jia, Y. Wang, A.N. Hong, C. Dang, H.E. Castillo, X. Bu, P. Feng, Pore-Space-Partition-Enabled Exceptional Ethane Uptake and Ethane-Selective Ethane-Ethylene Separation, J. Am. Chem. Soc. 142 (2020) 2222–2227.
[37] S.-M. Wang, H.-R. Liu, S.-T. Zheng, H.-L. Lan, Q.-Y. Yang, Y.-Z. Zheng, Control of pore structure by the solvent effect for efficient ethane/ethylene separation, Sep. Purif. Technol. 304 (2023), 122378.
[38] P.-Q. Liao, W.-X. Zhang, J.-P. Zhang, X.-M. Chen, Efficient purification of ethene by an ethane-trapping metal-organic framework, Nat. Commun. 6 (2015) 8697.
[39] H. Fang, B. Zheng, Z.-H. Zhang, H.-X. Li, D.-X. Xue, J. Bai, Ligand-Conformer-Induced Formation of Zirconium-Organic Framework for Methane Storage and MTO Product Separation, Angew. Chem. Int. Ed. 60 (2021) 16521–16528.
[40] B. Yu, S. Geng, H. Wang, W. Zhou, Z. Zhang, B. Chen, J. Jiang, A Solid Transformation into Carboxyl Dimers Based on a Robust Hydrogen-Bonded Organic Framework for Propyne/Propylene Separation, Angew. Chem. Int. Ed. 60 (2021) 25942–25948.
[41] Y. Chen, Z. Qiao, D. Lv, C. Duan, X. Sun, H. Wu, R. Shi, Q. Xia, Z. Li, Efficient adsorptive separation of C_3H_6 over C_3H_8 on flexible and thermoresponsive CPL-1, Chem. Eng. J. 328 (2017) 360–367.
[42] J. Pei, H.-M. Wen, X.-W. Gu, Q.-L. Qian, Y. Yang, Y. Cui, B. Li, B. Chen, G. Qian, Dense Packing of Acetylene in a Stable and Low-Cost Metal-Organic Framework for Efficient C_2H_2/CO_2 Separation, Angew. Chem. Int. Ed. 60 (2021) 25068–25074.
[43] O.T. Qazvini, R. Babarao, Z.-L. Shi, Y.-B. Zhang, S.G. Telfer, A Robust Ethane-Trapping Metal-Organic Framework with a High Capacity for Ethylene Purification, J. Am. Chem. Soc. 141 (2019) 5014–5020.
[44] H. Zeng, M. Xie, Y.-L. Huang, Y. Zhao, X.-J. Xie, J.-P. Bai, M.-Y. Wan, R. Krishna, W. Lu, D. Li, Induced Fit of C_2H_2 in a Flexible MOF Through Cooperative Action of Open Metal Sites, Angew. Chem. Int. Ed. 58 (2019) 8515–8519.
[45] J. Pires, M.L. Pinto, V.K. Saini, Ethane Selective IRMOF-8 and Its Significance in Ethane-Ethylene Separation by Adsorption, ACS Appl. Mater. Interfaces 6 (2014) 12093–12099.
[46] H.-G. Hao, Y.-F. Zhao, D.-M. Chen, J.-M. Yu, K. Tan, S. Ma, Y. Chabal, Z.-M. Zhang, J.-M. Dou, Z.-H. Xiao, G. Day, H.-C. Zhou, T.-B. Lu, Simultaneous Trapping of C_2H_2 and C_2H_6 from a Ternary Mixture of C_2H_2/C_2H_4/C_2H_6 in a Robust Metal-Organic Framework for the Purification of C_2H_4, Angew. Chem. Int. Ed. 57 (2018) 16067–16071.
[47] Z. Xu, X. Xiong, J. Xiong, R. Krishna, L. Li, Y. Fan, F. Luo, B. Chen, A robust Thazole framework for highly efficient purification of C_2H_4 from a C_2H_4/C_2H_2/C_2H_6 mixture, Nat. Commun. 11 (2020) 3163.
[48] W. Liang, F. Xu, X. Zhou, J. Xiao, Q. Xia, Y. Li, Z. Li, Ethane selective adsorbent Ni (bdc) $(ted)_{0.}$5 with high uptake and its significance in adsorption separation of ethane and ethylene, Chem. Eng. Sci. 148 (2016) 275–281.
[49] Y. Wu, H. Chen, D. Liu, Y. Qian, H. Xi, Adsorption and separation of ethane/ethylene on ZIFs with various topologies: Combining GCMC simulation with the ideal adsorbed solution theory (IAST), Chem. Eng. Sci. 124 (2015) 144–153.
[50] J. Pei, J.-X. Wang, K. Shao, Y. Yang, Y. Cui, H. Wu, W. Zhou, B. Li, G. Qian, Engineering microporous ethane-trapping metal-organic frameworks for boosting ethane/ethylene separation, J. Mater. Chem. A 8 (2020) 3613–3620.
[51] M. Kang, S. Yoon, S. Ga, D.W. Kang, S. Han, J.H. Choe, H. Kim, D.W. Kim, Y. G. Chung, C.S. Hong, High-Throughput Discovery of $Ni(IN)_2$ for Ethane/Ethylene Separation, Adv. Sci. 8 (2021) 2004940.
[52] H. Lyu, J. Zhu, B. Zhou, H. Cao, J. Duan, L. Chen, W. Jin, Q. Xu, Structure-directed fabrication of ultrathin carbon nanosheets from layered metal salts: A separation and supercapacitor study, Carbon 139 (2018) 740–749.
[53] W. Fan, Y. Wang, Q. Zhang, A. Kirchon, Z. Xiao, L. Zhang, F. Dai, R. Wang, D. Sun, An Amino-Functionalized Metal-Organic Framework, Based on a Rare $Ba_{12}(COO)_{18}(NO_3)_2$ Cluster, for Efficient C_3/C_2/C_1 Separation and Preferential Catalytic Performance, Chem.-Eur. J. 24 (2018) 2137–2143.
[54] L. Zhang, L.-N. Ma, G.-D. Wang, L. Hou, Z. Zhu, Y.Y. Wang, A new honeycomb MOF for C_2H_4 purification and C_3H_6 enrichment by separating methanol to olefin products, J. Mater. Chem. A 11 (2023) 2343–2348.
[55] D. Geng, M. Zhang, X. Hang, W. Xie, Y. Qin, Q. Li, Y. Bi, Z. Zheng, A 2D metal-thiacalix[4]arene porous coordination polymer with 1D channels: gas absorption/separation and frequency response, Dalton Trans. 47 (2018) 9008–9013.
[56] R. Krishna, Screening metal-organic frameworks for mixture separations in fixed-bed adsorbers using a combined selectivity/capacity metric, RSC Adv. 7 (2017) 35724–35737.
[57] R. Krishna, Methodologies for screening and selection of crystalline microporous materials in mixture separations, Sep. Purif. Technol. 194 (2018) 281–300.
[58] R. Krishna, Metrics for Evaluation and Screening of Metal-Organic Frameworks for Applications in Mixture Separations, ACS Omega 5 (2020) 16987–17004.
[59] X. Zhang, L. Li, J.-X. Wang, H.-M. Wen, R. Krishna, H. Wu, W. Zhou, Z.-N. Chen, B. Li, G. Qian, B. Chen, Selective Ethane/Ethylene Separation in a Robust Microporous Hydrogen-Bonded Organic Framework, J. Am. Chem. Soc. 142 (2020) 633–640.

Supporting Information

A Separation MOF with O/N Active Sites in Nonpolar Pore for One-step C_2H_4 Purification from C_2H_6 or C_3H_6 Mixtures

Yong-Zhi Li[a], Gang-Ding Wang[b], Rajamani Krishna[c], Qing Yin[a], Danyang Zhao[a], Jiqiu Qi [a], Yanwei Sui[a]*, and Lei Hou[b]*

[a]School of Materials and Physics, China University of Mining and Technology, Xuzhou 221116, P. R. China

[b]Key Laboratory of Synthetic and Natural Functional Molecule of the Ministry of Education, College of Chemistry & Materials Science, Northwest University, Xi'an 710069, P. R. China.

[c]Van 't Hoff Institute for Molecular Sciences, University of Amsterdam 1098 XH Amsterdam (The Netherlands)

*To whom correspondence should be addressed. E-mail: lhou2009@nwu.edu.cn (Lei Hou); wyds123456@outlook (Yanwei Sui).

Materials and general methods

All solvents and organic ligand for synthesis were purchased commercially from The Shanghai Tensus Bio-tech Co., Ltd. Elemental analyses of C, H, and N were determined with a Perkin-Elmer 2400C elemental analyzer. Thermalgravimetric analyses (TGA) were carried out in a nitrogen stream using a Netzsch TG209F3 equipment at a heating rate of 10 °C min^{-1}. Single crystal diffraction data were collected on a Bruker SMART APEX II CCD single crystal diffractometer. Gas adsorption measurements were performed with an automatic volumetric sorption apparatus (Micrometrics ASAP 2020M). Water sorption was collected by Quantachrome Vstar vapor adsorption equipment. Breakthrough experiments were performed on a Quantachrome dynaSorb BT equipments.

X-Ray Crystallography

A Bruker Smart Apex II CCD detector was used to collect the single crystal data at 216(2) K using Mo Kα radiation (λ = 0.71073 Å). The structure was solved by direct methods and refined by full-matrix least-squares refinement based on F^2 with the Olex 2 program. The non-hydrogen atoms were refined anisotropically with the hydrogen atoms added at their geometrically ideal positions and refined isotropically. As the disordered solvent molecules in the structure cannot be located, the SQUEEZE routine of Platon program was applied in refining. The formula of complex was got by the single crystal analysis together with elemental microanalyses and TGA data. Relevant crystallographic results are listed in Table S1. Selected bond lengths and angles are provided in Table S2.

N_2 Sorption Isotherm

Before gas sorption experiments, All the as-synthesized samples were immersed in acetone for 3 days, during which the solvent was decanted and freshly replenished three times a day. All the samples were activated under vacuum at 333 K for 4 hours to obtain activated **1a**. Gas sorption measurements were then conducted using a Micrometrics ASAP 2020M gas adsorption analyzer.

Transient breakthrough simulations

Transient breakthrough simulations were carried out for the same set of operating conditions as in the experimental data sets, using the methodology described in earlier publications.[1-5] In

these simulations, intra-crystalline diffusion influences are ignored. For **1a**, there is excellent match between the experiments and simulations. From the breakthrough simulations, the productivities of 99.9% pure C_2H_4 were determined; these are expressed in the units of L per kg of **1a**.

Breakthrough Experiments

The breakthrough experiment was performed on the Quantachrome dynaSorb BT equipments at 298 K and 1 bar with an equal volume of mixed gas (gas A: gas B: Ar = 5% : 5% : 90%, Ar as the carrier gas, flow rate = 5 mL min^{-1}). The activated MOF (1 g) was filled into a packed column of ϕ 4.2×80 mm, and then the packed column was washed with Ar at a rate of 7 mL min^{-1} at 333 K for 35 minutes to further activate the samples. Between two breakthrough experiments, the adsorbent was regenerated by Ar flow of 7 mL min^{-1} for 35 min at 333 K to guarantee a complete removal of the adsorbed gases.

GCMC Simulation

Grand canonical Monte Carlo (GCMC) simulations were performed for the gas adsorption in the framework by the Sorption module of Material Studio (Accelrys. Materials Studio Getting Started, release 5.0). The framework was considered to be rigid, and the optimized gas and epoxide molecules were used. The partial charges for atoms of the framework were derived from QEq method and QEq neutral 1.0 parameter. One unit cell was used during the simulations. The interaction energies between the gas molecules and framework were computed through the Coulomb and Lennard-Jones 6-12 (LJ) potentials. All parameters for the atoms were modeled with the universal force field (UFF) embedded in the MS modeling package. A cutoff distance of 12.5 Å was used for LJ interactions, and the Coulombic interactions were calculated by using Ewald summation. For each run, the 5×10^6 maximum loading steps, 5×10^6 production steps were employed.

Fitting of experimental data on pure component isotherms

The unary isotherm data for C_2H_4, C_2H_6, and C_3H_6, measured at two different temperatures 273 K, and 298 K in **1a** were fitted with good accuracy using the dual-site Langmuir-Freundlich model, where we distinguish two distinct adsorption sites A and B:

$$q = \frac{q_{sat,A} b_A p^{\nu A}}{1 + b_A p^{\nu A}} + \frac{q_{sat,B} b_B p^{\nu B}}{1 + b_B p^{\nu B}} \quad \text{(S1)}$$

In eq (S1), the Langmuir-Freundlich parameters b_A, b_B are both temperature dependent

$$b_A = b_{A0} \exp\left(\frac{E_A}{RT}\right); \quad b_b = b_{B0} \exp\left(\frac{E_B}{RT}\right) \quad \text{(S2)}$$

In eq (S2), E_A, E_B are the energy parameters associated with sites A, and B, respectively.

The fit parameters are provided in Table S,

Isosteric heat of adsorption

The isosteric heat of adsorption, Q_{st}, is defined as

$$Q_{st} = -RT^2 \left(\frac{\partial \ln p}{\partial T}\right)_q \quad \text{(S3)}$$

where the derivative in the right member of eq (S3) is determined at constant adsorbate loading, q. The derivative was determined by analytic differentiation of the combination of eq (S1), eq (S2), and eq (S3).

Gas Selectivity Prediction via IAST

The experimental isotherm data for pure C_2H_4, C_2H_6 and C_3H_6 were fitted using a dual Langmuir-Freundlich (L-F) model:

$$q = \frac{a_1 * b_1 * P^{c_1}}{1 + b_1 * P^{c_1}} + \frac{a_2 * b_2 * P^{c_2}}{1 + b_2 * P^{c_2}}$$

Where q and p are adsorbed amounts and the pressure of component i, respectively.

The adsorption selectivities for binary mixtures, defined by

$$S_{i/j} = \frac{x_i * y_j}{x_j * y_i}$$

Were respectively calculated using the Ideal Adsorption Solution Theory (IAST). Where xi is the mole fraction of component i in the adsorbed phase and yi is the mole fraction of component i in the bulk.

Molecular structure						
Molecular formula	Molecular Dimension (Å)			Kinetic diameter (Å)	Polari × 10^{-25} (cm^{-3})	Boiling point(K)
	X	*Y*	*Z*			
C_2H_4	3.28	4.18	4.84	4.16	42.5	169.4
C_2H_6	3.81	4.08	4.82	4.44	44.3-44.7	184.6
C_3H_6	4.20	5.30	6.40	4.68	62.6	225.5

Scheme S1. Structures and physical properties of C_2H_4, C_2H_6 and C_3H_6.

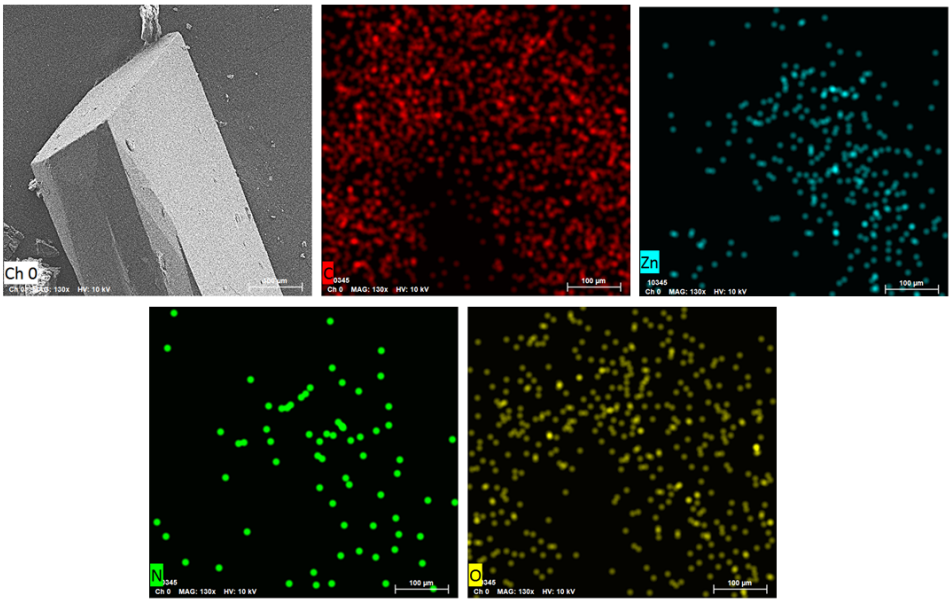

Figure S1. SEM images of as-synthesized MOF, and elemental mapping from SEM-EDX showing uniform distribution of elements (mixed elements, C, Zn, N, O) in the selected area of crystal.

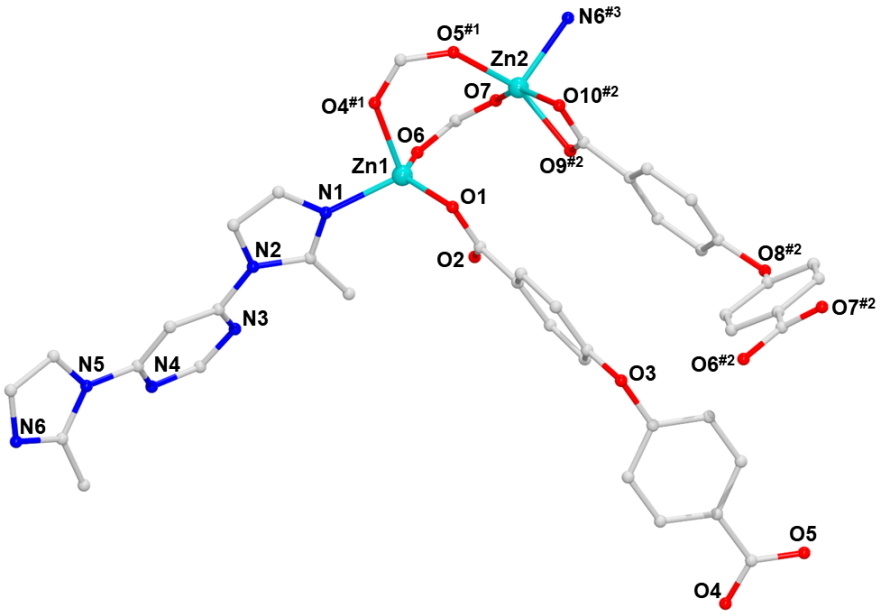

Figure S2. Coordination environment of Zn(II) ions.

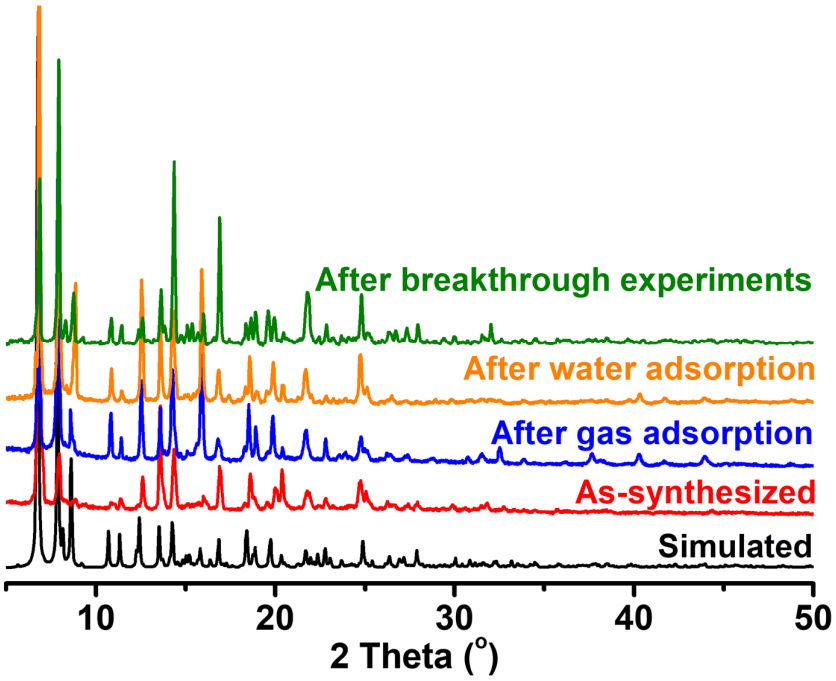

Figure S3. PXRD patterns of **1**.

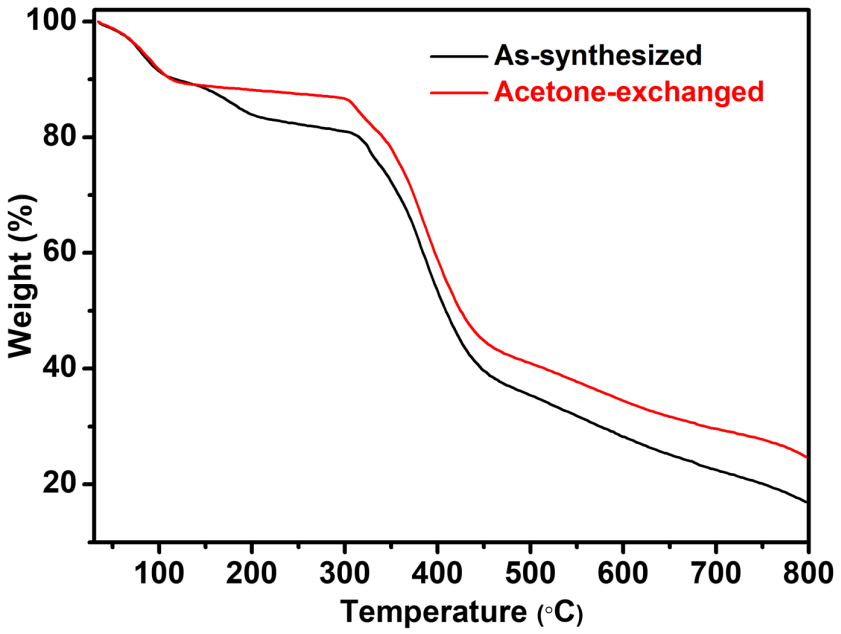

Figure S4. TGA curves of as-synthesized and acetone-exchanged samples of **1**.

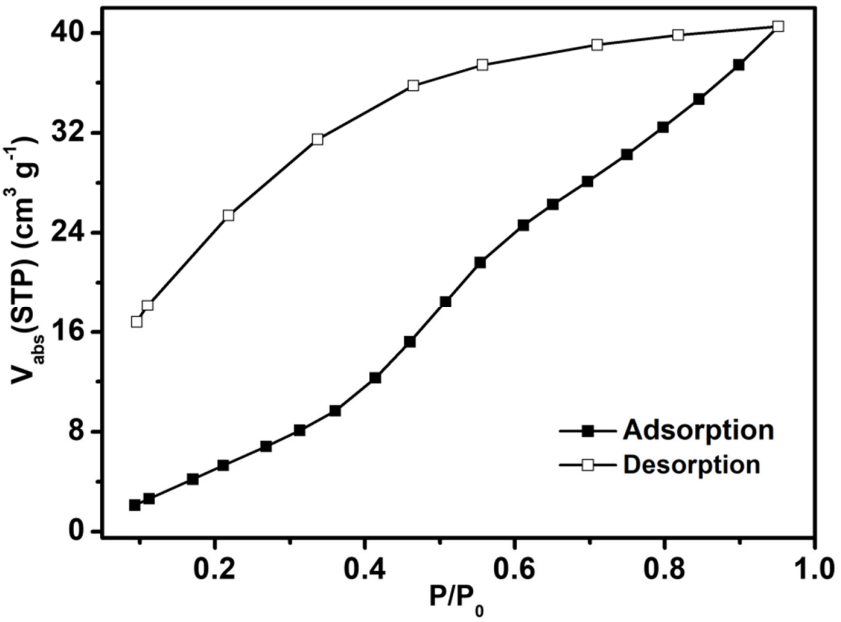

Figure S5. Water vapor adsorption and desorption isotherm of **1a** at 298 K.

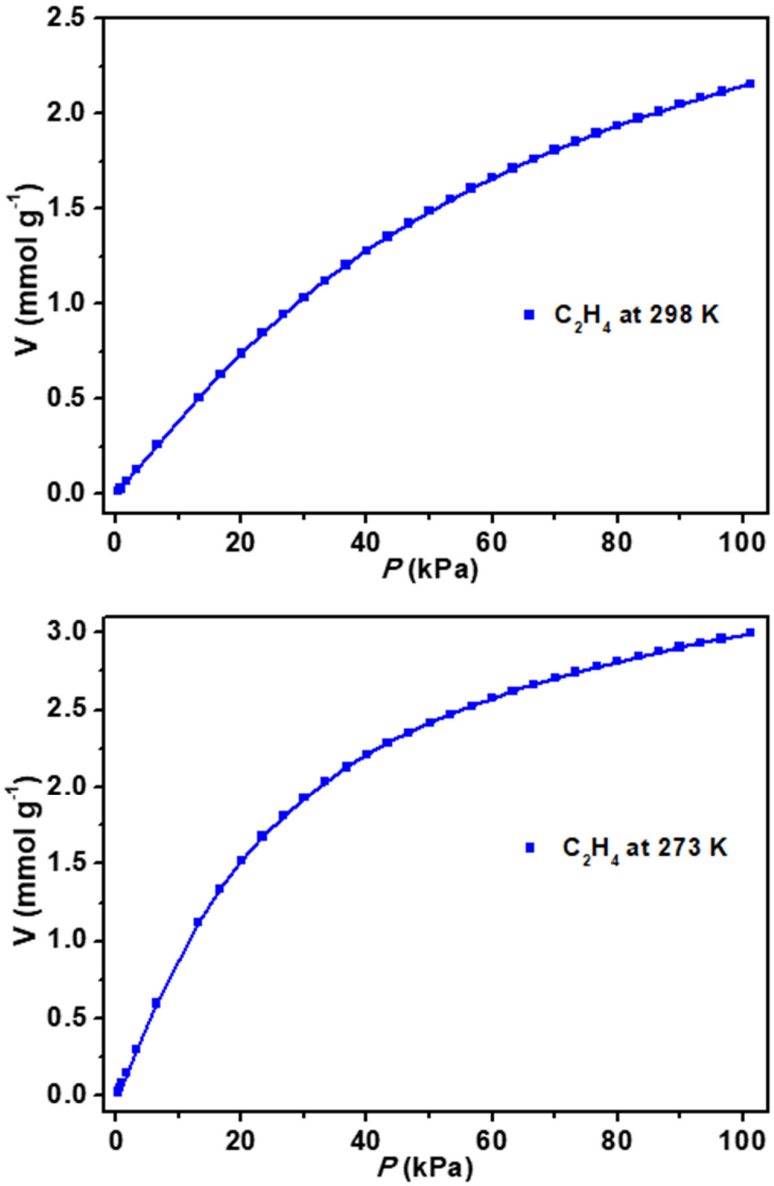

Figure S6. C_2H_4 adsorption isotherms of **1a** with fitted by dual L-F model at 298 K and 273 K, 298 K: a1 = 3.43606, b1 = 0.00921, c1 = 1.12333, a2 = 0.01901, b2 = 0.6084, c2 = 1.18178, Chi^2 = 3.4532E-7, R^2 =1; 273 K: a1 = 3.52331, b1 = 0.02478, c1 = 1.14267 a2 = 0.17732, b2 = 2.1274E-9, c2 = 4.25404, Chi^2 = 0.00002, R^2 = 0.99999.

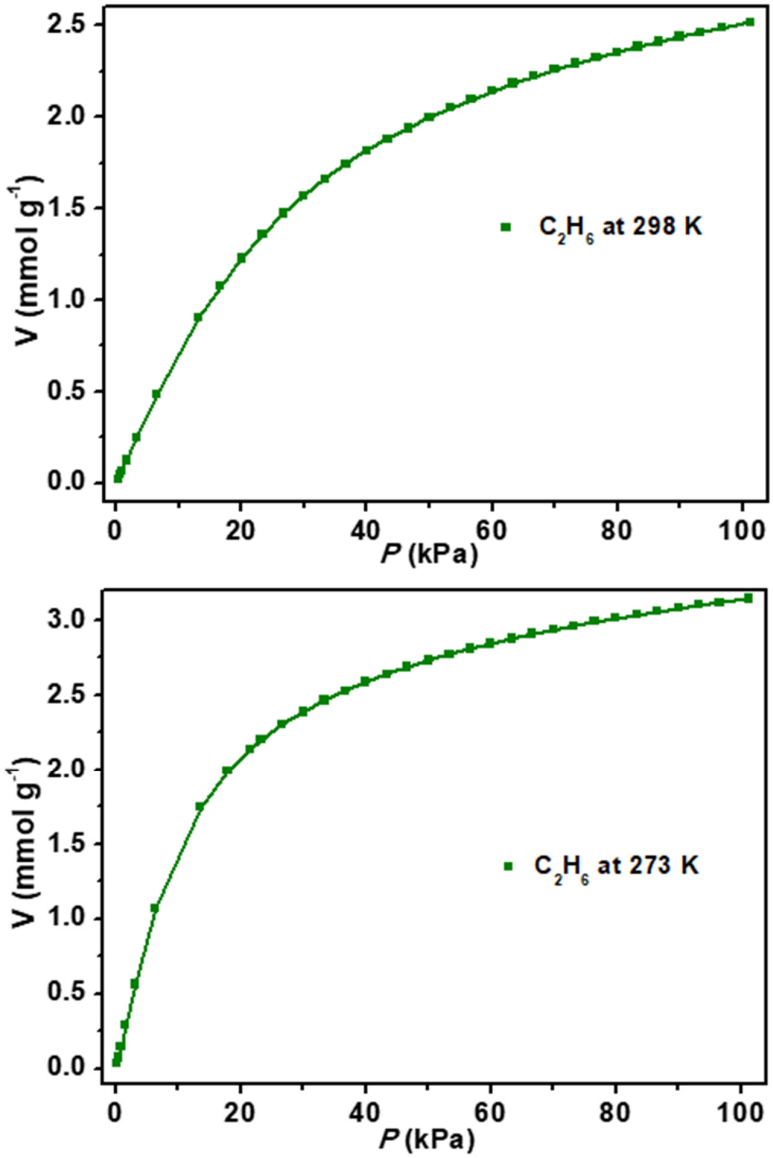

Figure S7. C_2H_6 adsorption isotherms of **1a** with fitted by dual L-F model at 298 K and 273 K, 298 K: a1 = 3.06171, b1 = 0.02323, c1 = 1.12105, a2 = 0.09758, b2 = 2.3658E-9, c2 = 4.34811, Chi^2 = 8.1286E-6, R^2 = 0.99999; 273 K: a1 = 2.97636, b1 = 0.05995, c1 = 1.20031, a2 = 0.8132, b2 = 0.00025, c2 = 1.73607, Chi^2 = 0.00003, R^2 = 0.99998.

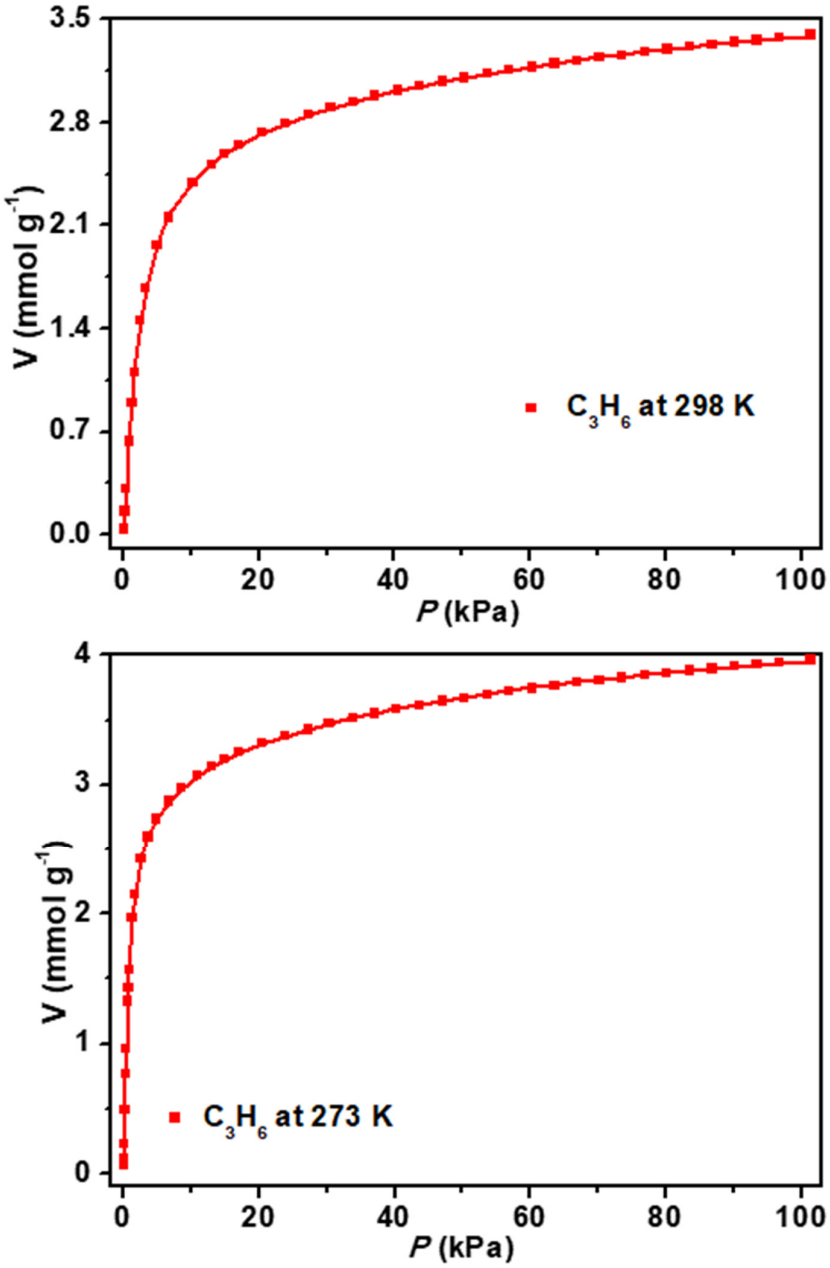

Figure S8. C_3H_6 adsorption isotherms of **1a** with fitted by dual L-F model at 298 K and 273 K, 298 K: a1 = 2.60175, b1 = 0.38696, c1 = 1.20055, a2 = 1.34085, b2 = 0.01105, c2 = 1.06743, Chi^2 = 0.00002, R^2 = 0.99998; 273 K: a1 = 2.6841, b1 = 0.10486, c1 = 0.59355, a2 = 2.29332, b2 = 1.83345, c2 = 1.41842, Chi^2 = 0.00004, R^2 = 0.99997.

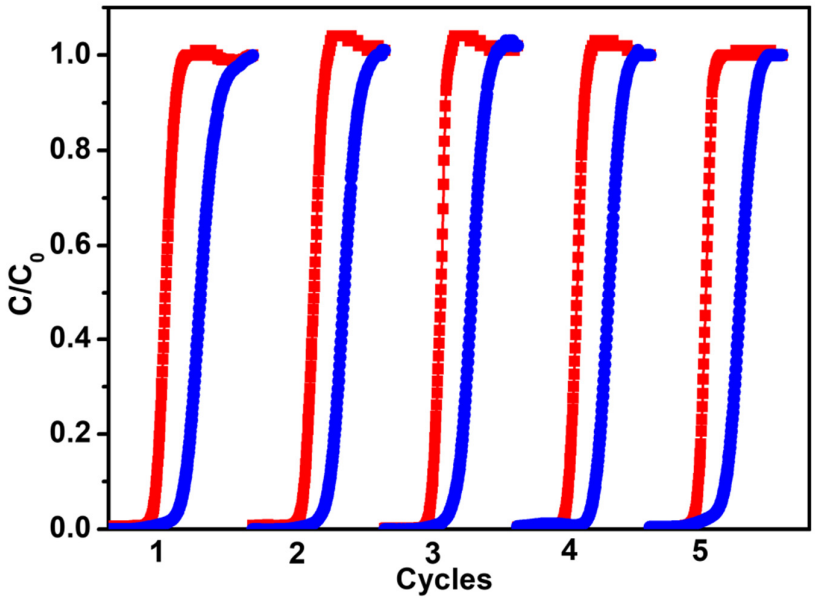

Figure S9. Cycling tests for equimolar C_2H_6/C_2H_4 mixture at 298 K.

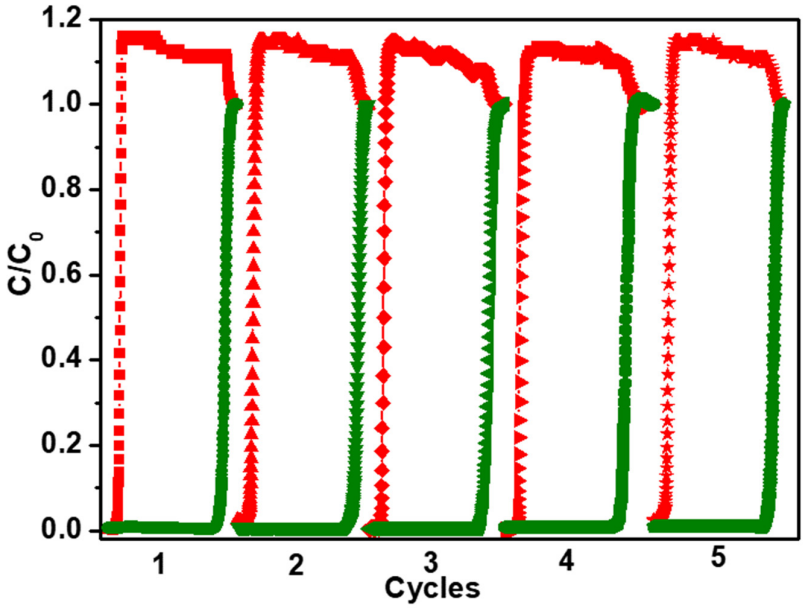

Figure S10. Cycling tests for equimolar C_3H_6/C_2H_4 mixture at 298 K.

Table S1. Crystal Data and Structure Refinements for **1**.

Chemical formula	$C_{40}H_{28}Zn_2N_6O_{10}$
Formula weight	883.42
T (K)	216(2)
Crystal system, Space group	Triclinic, *P-1*
a (Å)	13.0194(4)
b (Å)	14.4119(4)
c (Å)	16.3911(4)
α (°)	87.5590(10)
β (°)	72.9610(10)
γ (°)	65.3030(10)
V (Å^3)	2660.26(13)
Z	2
$D_{calcd.}$[g·cm^{-3}]	1.103
μ (mm^{-1})	0.950
Reflns collected/unique/R_{int}	42527/9700/0.0369
Goof	1.051
R_1^a, wR_2^b [I > 2σ]	R_1 = 0.0367, wR_2 = 0.1055
R_1^a, wR_2^b (all data)	R_1 = 0.0482, wR_2 = 0.1118

$^a R_1 = \Sigma(|F_o|-|F_c|)/\Sigma|F_o|$. $^b R_2 = [\Sigma w(F_o^2 - F_c^2)^2/\Sigma w(F_o^2)^2]^{1/2}$.

Table S2. Selected bond lengths [Å] and angles [°] for **1**.

Zn(1)-O(5)	1.9501(18)	O(5)-Zn(1)-N(6)#3	99.62(8)
Zn(1)-O(7)#1	1.9801(19)	O(7)#1-Zn(1)-N(6)#3	98.29(9)
Zn(1)-O(10)#2	1.9576(18)	O(10)#2-Zn(1)-O(7)#1	103.77(8)
Zn(1)-N(6)#3	2.033(2)	O(10)#2-Zn(1)-N(6)#3	106.41(8)
Zn(2)-O(1)	1.9384(19)	O(1)-Zn(2)-O(4)#4	104.17(8)
Zn(2)-O(4)#4	1.9952(19)	O(1)-Zn(2)-O(6)	130.37(9)
Zn(2)-O(6)	1.9404(19)	O(1)-Zn(2)-N(1)	115.05(9)
Zn(2)-N(1)	2.007(2)	O(4)#4-Zn(2)-N(1)	96.21(8)
O(5)-Zn(1)-O(7)#1	106.20(8)	O(6)-Zn(2)-O(4)#4	101.75(9)
O(5)-Zn(1)-O(10)#2	136.55(8)	O(6)-Zn(2)-N(1)	103.19(9)

Symmetry codes: #1 x, y+1,z; #2 x-1, y+2, z; #3 x,y+1,z; #4 x, y-1, z; #5 x+1, y-2, z; #6 x, y-1, z+1.

Table S3. Dual-site Langmuir-Freundlich fits for C_2H_4, C_2H_6, and C_3H_6, in **1a**.

	Site A				Site B			
	$\frac{q_{A.sat}}{\text{mol kg}^{-1}}$	$\frac{b_{A,0}}{\text{Pa}^{-\nu_A}}$	$\frac{E_A}{\text{kJ mol}^{-1}}$	ν_A	$\frac{q_{B.sat}}{\text{mol kg}^{-1}}$	$\frac{b_{B,0}}{\text{Pa}^{-\nu_B}}$	$\frac{E_B}{\text{kJ mol}^{-1}}$	ν_B
C_2H_4	2.2	1.951E-09	24	0.83	2.1	7.38E-12	30	1.25
C_2H_6	2.2	7.684E-09	23.3	0.75	2	6.65E-12	31.5	1.3
C_3H_6	2.1	2.855E-13	44.5	1.44	2.6	5.45E-08	24	0.61

References

S1 R. Krishna, The Maxwell-Stefan Description of Mixture Diffusion in Nanoporous Crystalline Materials, *Microporous Mesoporous Mater.* **2014**, 185, 30-50.

S2 R. Krishna, Methodologies for Evaluation of Metal-Organic Frameworks in Separation Applications, *RSC Adv.* **2015**, 5, 52269-52295.

S3 R. Krishna, Screening Metal-Organic Frameworks for Mixture Separations in Fixed-Bed Adsorbers using a Combined Selectivity/Capacity Metric, *RSC Adv*. **2017**, 7, 35724-35737.

S4 R. Krishna, Methodologies for Screening and Selection of Crystalline Microporous Materials in Mixture Separations, *Sep. Purif. Technol*. **2018**, 194, 281-300.

S5 R. Krishna, Metrics for Evaluation and Screening of Metal-Organic Frameworks for Applications in Mixture Separations, *ACS Omega* **2020**, 5, 16987-17004.